Bioprocess and Biosystems Engineering (2024) 47:65–74
https://doi.org/10.1007/s00449-023-02945-7

RESEARCH PAPER

Papaya peel extract-mediated green synthesis of zinc oxide nanoparticles and determination of their antioxidant, antibacterial, and photocatalytic properties

Serina Easmin[1] · Moulik Bhattacharyya[1] · Krishna Pal[1] · Priya Das[1] · Ranabir Sahu[1] · Gouranga Nandi[1] · Saikat Dewanjee[2] · Paramita Paul[1] · Md Salman Haydar[3] · Swarnendu Roy[3] · Tarun Kumar Dua[1]

Received: 21 September 2023 / Accepted: 8 November 2023 / Published online: 12 December 2023

Abstract

This study describes an effective and eco-friendly approach to the synthesis of zinc oxide nanoparticles (ZnONPs) utilizing papaya fruit peel extract (PPE). The structural evaluation and morphological features of synthesized ZnONPs were examined using various physicochemical analyses. The formulated ZnONPs were spherical to hexagonal in shape with ~ 170 nm in diameter. ZnONPs exhibited improved antioxidant potential in terms of DPPH radical scavenging activity (IC_{50} = 98.74 µg/ml) and ferric-reducing potential compared with PPE. The antibacterial activity of ZnONPs was measured against pathogenic strains of *Salmonella typhi, Bacillus subtilis, Staphylococcus aureus,* and *Escherichia coli*. The biosynthesized ZnONPs showed potential antibacterial efficacy against all microbes. In addition, ZnONPs exhibited potential photocatalytic activity in rhodamine B degradation in the presence of sunlight. The results indicated that papaya peels, which are these fruit wastes, could be helpful for the green synthesis of ZnONPs with good dose-responsive antioxidant, antibacterial, and photocatalytic activities.

Graphical abstract

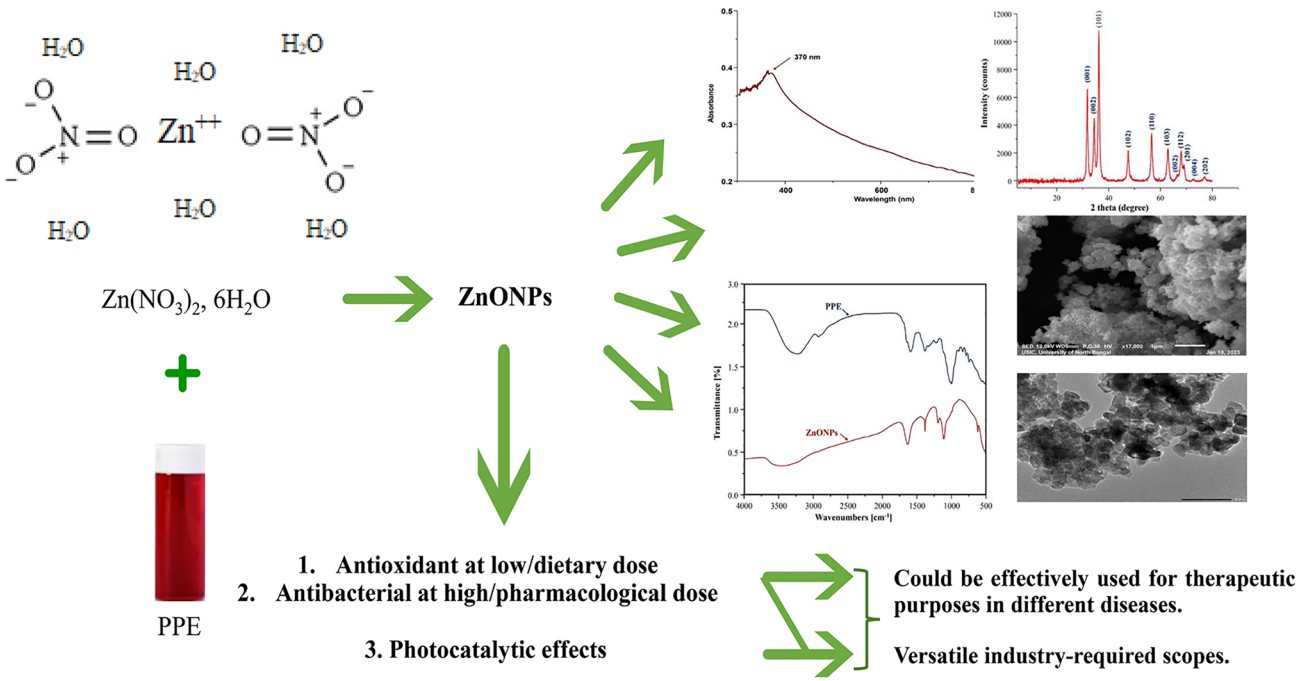

Extended author information available on the last page of the article

Keywords Antibacterial activity · Green synthesis · Papaya peel extract · Photocatalytic activity · ZnONPs

Introduction

Metal oxides are snatching the spotlight in research because of their appealing physicochemical, electrical, and optical properties. They can be formulated into nano-scaled particles with diverse attributes, including high reactivity, definite surface area, and controllable size [1, 2]. Zinc oxide (ZnO) is one of the known metal oxides that has attracted much attention recently because of its unique and attractive features in various fields, including chemistry, physics, biology, medicine, and electronics [3, 4]. Therefore, there is increasing interest in producing ZnO-derived nanoparticles [1, 5]. These nanoparticles are widely used in calamine lotions, baby powders, ceramics, UV filters, ointments, paints, food additives, and other products [4, 6]. Additionally, it has been claimed that ZnO-derived nanoparticles may have positive effects on human health, including antibacterial, antioxidant, anticorrosive, and anticancer activities [4, 7–9]. However, the expense and production of hazardous waste make the synthesis of ZnO-derived nanoparticles undesirable via chemical and physical processes [10–12]. Based on the advanced green synthesis approach, plant extracts are used as a central component for nanoparticle synthesis, which has the potential to be advantageous since they are quick, easy, less energy-intensive, less waste producing, and ecologically benign. These make it possible to manufacture the appropriate distribution of metal oxide nanoparticles using an affordable synthesis process [1, 13, 14]. According to scientific reports, biomolecules and secondary metabolites found in plant extracts, such as tannins, flavonoids, saponins, polyphenols, alkaloids, and terpenoids, are responsible for the efficient reduction of zinc precursors [15, 16]. Furthermore, compared to other environmentally friendly biological methods, using agricultural wastes, such as peel extracts, to create nanoparticles has additional advantages. Fruit peels are incredibly abundant in bioactive substances that can be employed as antibacterial and antioxidant agents. The by-products of the food and beverage industry are either discarded or given to animals. However, the current research on fruit peels is following a trend to find a practical approach to extract bioactive chemicals with antioxidant and antibacterial characteristics from the fruit peels to improve health development [17].

Several members of the Caricaceae family, including *Carica papaya,* have been used as remedies for a variety of illnesses. Numerous scientific investigations have evaluated the biological properties of different *Carica papaya* sections, including fruits, shoots, leaves, rinds, peel, seeds, roots, and latex [18]. Papain and chymopapain, two phytoenzymes found in *Carica papaya*, are frequently used to treat digestive issues [17]. Various portions of *Carica papaya* have been claimed to have therapeutic effects, including anti-hypertensive, antibacterial, diuretic, anti-fertility, anti-fungal, and anticancer activities. Papaya leaf and fruit extract has antibacterial and antioxidant properties because they contains phenols, vitamins, and enzymes [19–21]. It has also shown potential activity to cure dengue fever [22]. In the present study, *Carica papaya* peel extract was used as a reducing agent in the biological fabrication of ZnO-derived nanoparticles (ZnONPs). The crystal structure, surface morphology, and size were identified using UV–visible spectroscopic, Fourier transform infrared (FTIR) spectroscopic, scanning electron microscopic (SEM), transmission electron microscopic (TEM), energy-dispersive X-ray (EDX) spectroscopic, and dynamic light scattering (DLS) analyses. The efficacy of ZnONPs as photocatalysts in terms of the breakdown of rhodamine B in the presence of sunlight, as antioxidants in terms of DPPH (2,2-diphenyl-1-picrylhydrazyl) radical scavenging potential and FRAP (ferric ion-reducing antioxidant power) and as antibacterial agents against Gram-positive and Gram-negative bacteria were determined.

Materials and methods

Materials

Chemicals used in this study, including di-sodium hydrogen phosphate (Na_2HPO_4), trichloroacetic acid (CCl_3COOH), dibasic sodium salt (NaH_2PO_4), and sodium hydroxide (NaOH), were obtained from Himedia, Mumbai, India. All of the solvents utilized in the present study were analytical grade and procured from Merck, Mumbai, India. Other important chemicals, such as DPPH, potassium ferricyanide ($K_3[Fe(CN)_6]$), and rhodamine B, were bought from Sisco Research Laboratories, Mumbai, India. Various standard compounds including ascorbic acid and zinc nitrate hexahydrate were obtained from Sigma-Aldrich, Bangalore, India.

Collection and preparation of papaya peel extract

The *Carica papaya (C. papaya)* fruits were collected from local markets of Siliguri, India. Then fruits were washed thoroughly with distilled water to remove dust particles. The peels were taken of and cut into small pieces. Then the chopped peels were dried at 40 °C in a hot air oven. Further, dried peels were powdered in a mixer grinder. Afterward,

5 g of peel powder was extracted with 100 ml distilled water at 60 °C for 60 min. Finally, the menstruum was filtered by using Whatman No.1 filter paper to obtain aqueous extract of papaya peel (PPE) and was stored in refrigerator for further use [23].

Preparation of ZnONPs

The ZnONPs were synthesized by using PPE. Briefly, 10 ml of PPE was added to the 90 ml of 0.1 M ($Zn(NO_3)_2$, $6H_2O$) solution in a beaker and mixture was then agitated continuously at 60 °C using a magnetic stirrer. The pH of the resulting solution was then subsequently raised to 8 using NaOH solution. The transition of the solution's color from dark red to pale white (Fig. 1) indicated the formation of ZnONPs. The particles were separated after one hour by centrifuging those around 16,000 rpm for 15 min. After that, the supernatant was decanted and ZnONPs were washed with ethanol for 3 times to eliminate the contaminants. The sample identified as ZnONPs was heated in the furnace for 2 h at 400 °C [24] and the powdered ZnONPs were stored for further analysis.

Characterization of ZnONPs

UV–visible spectrum of ZnONPs

The synthesis of ZnONPs was evaluated by using a UV–visible spectrophotometer (UV-1780, Shimadzu, Japan). The spectrum was obtained at a resolution of 1 nm in the 300 to 800 nm wavelength range using distilled water as blank [24].

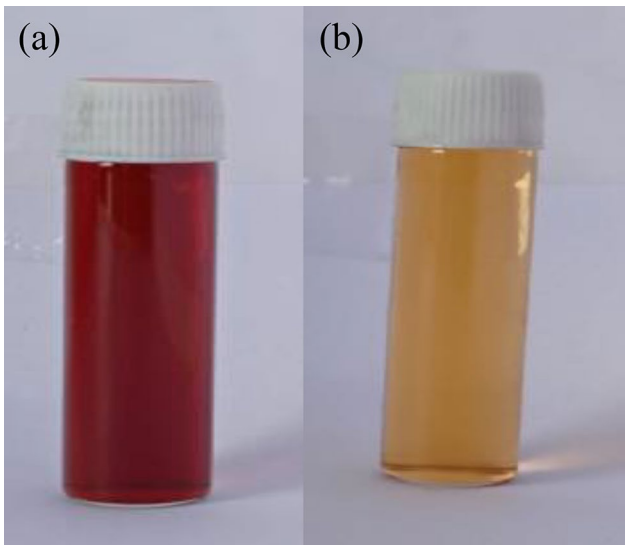

Fig. 1 The color transition of PPE (**a**) after formation of ZnONPs (**b**)

FTIR analysis of ZnONPs

The FTIR analysis was done by using pellet techniques where potassium bromide (KBr) was used as a carrier [25]. The IR spectrum was recorded by operating the Alpha II FTIR (Bruker Optik GmbH, Ettlingen, Germany) equipment in the 4000 to 500 cm^{-1} frequency region.

XRD analysis of ZnONPs

The crystallographic profile of ZnONPs was analyzed using (XRD, Bruker D8 using TOPAS 4.2 software, Germany) with Zn Kα radiation source ($\lambda = 50.1546$ nm) at 15 kV and 50 mA for determination of diffractogram pattern. The scan speed was 2°/min and the spectra of 2θ (Bragg angle) were recorded in the range of 5° to 80° [26].

Particle size and zeta potential analysis of ZnONPs

The hydrodynamic diameters and zeta potential of ZnONPs were determined by using a DLS instrument Litesizer 500 (Anton Paar, Graz, Austria). Briefly, a very small quantity of sample was added to milli-Q water and sonicated. The particle size and zeta potential were measured using PVC and omega cuvettes, respectively [27].

SEM of ZnONPs

The morphological characteristics of the ZnONPs were investigated using a JEOL, JSM-IT100 Scanning electron microscope (Tokyo, Japan) [28]. In order to make the dried sample conductive, the sample was mounted on a metal stub and sputtered with gold. Images of 17000 × magnification obtained at a voltage of 12 kV demonstrated the nanostructure of the particles.

TEM of ZnONPs

The shape and size of sample were examined by TEM (JEOL JEM-2100 Plus, Tokyo, Japan). The copper grid was coated with a thin coating of the ZnONPs solution for TEM examination. The pictures were captured after drying the grid [29].

EDX of ZnONPs

The presence of elements in synthesized ZnONPs was evaluated by using EDX. The presence of metals in sample was ensured by analyzing the peak emission resulting from

the interaction between metal and X-ray beam. Generally, each element has a unique atomic pattern allowing a different peaks for its electromagnetic emission spectrum [30].

In vitro antioxidant assay of ZnONPs

DPPH radical scavenging activity of ZnONPs

Antioxidant activity of PPE and green synthesized ZnONPs were assessed by performing the DPPH radical scavenging assay [31]. Briefly, the stock solutions of PPE, ZnONPs, and a standard antioxidant (ascorbic acid) were made separately by dissolving 1 mg of individual sample in methanol (1 ml). Then different dilutions of the stock solutions were treated with 1 ml of a 0.3 mM DPPH solution. The reaction mixture was then allowed to incubate for 30 min at room temperature in the dark. The absorbance (Abs) was then determined at 517 nm using 1 ml of DPPH solution as a control and methanol as a blank. The following formula was used to determine the DPPH radical scavenging activity:

$$\text{Percentage of DPPH scavenging activity } (\%inhibition) = \frac{\text{Abs(c)} - \text{Abs(s)}}{\text{Abs(c)}} \times 100.$$

The Abs of the control is Abs(c), and the Abs of the sample is Abs(s). The percentage of inhibition against concentration (µg/ml) was plotted and the IC_{50} was reported.

FRAP of ZnONPs

The reducing power assay of PPE and ZnONPs was calculated as per the method described by Oyaizu [32] with some modifications. The stock solutions of PPE, ZnONPs, and ascorbic acid were prepared at a concentration of 1 mg/ml in purified water. Different dilutions of stock solutions were treated with 2.5 ml of 0.2 M phosphate buffer (pH 6.6) and 2.5 ml of 1% potassium ferricyanide and incubated for 25 min at 50 °C on a water bath. After incubation, the solution was allowed to cool before being treated with 2.5 ml of 10% trichloroacetic acid and vortexed for proper mixing. 2.5 ml of the resulting solution was pipetted from the aforementioned mixture and diluted with 2.5 ml of purified water. Finally, 0.5 ml of 0.1% ferric chloride was added. The absorbance of resulting solutions was checked at 700 nm against phosphate buffer as the blank solution.

Antibacterial activity of ZnONPs

Using the disc diffusion method, antibacterial activity was evaluated against two Gram-positive and two Gram-negative bacterial strains [33]. Gram-positive *Bacillus subtilis* ATCC 11774 and *S. aureus* ATCC 11632 strains and Gram-negative *Salmonella typhimurium* ATCC 25241 and *Escherichia coli* ATCC 11229 strains were chosen for this assay. The selected bacterial strains were grown on nutrient broth to obtain fresh viable cells. The test organisms were placed on a nutrient agar plate, stirred thoroughly, and hardened. After that, the filter paper discs, previously soaked with the 500 µg/ml of PPE and ZnONPs, were placed on the agar surface. Antibacterial efficacy was assessed by measuring the diameter of the disk-encircling inhibited zone using a millimeter scale. Streptomycin (500 µg/ml) was used as positive control.

Further, the minimum inhibitory concentration (MIC) was also assessed to confirm the potent antibacterial activity of synthesized ZnONPs. The culture was maintained at 10^6 CFU/ml by adding 100 µl of actively growing viable cells, various doses of ZnONPs, and 50 ml sterilized nutrient broth. Using a Systronics double beam spectrophotometer-2201 (Ahmedabad, India), microbial growth was assessed at 600 nm after 24 h of incubation (at 120 rpm and 37 °C). The MIC value of standard antibiotics and PPE was also evaluated following the same protocols.

Photocatalytic activity of ZnONPs

Rhodamine degradation capacity under solar exposure in the presence of a substance determines the photocatalytic property of this substance. In this study, exactly 0.75 mg of rhodamine B was dissolved in 150 ml of distilled water and sonicated to generate a dye solution. Then, 15 mg of PPE and ZnONPs was added into the 25 ml of rhodamine B dye solution and stirred for 30 min under shade followed by solar irradiation exposure to the colloidal suspension. During the experiment, the average atmospheric temperature was found to be 30 °C with a shine duration of 3 h. To compare any changes in the coloration, a control was also preserved under the identical circumstances but without the addition of nanoparticles. At every 30 min, 3 ml of suspension was collected from the colloidal mixer. The collected suspension sample was scanned spectrophotometrically from 300 to 800 nm to study the degradation of rhodamine B. The results were calculated as dye degradation (%) using the following equation [34].

$$\text{Dye degradation } (\%) = \frac{c_0 - c_t}{c_0} \times 100.$$

Here c_0 is the initial concentration and c_t is the concentration after being exposed to irradiation for specific time (t) of rhodamine B.

Statistical analysis

The experimental findings are represented as the mean ± standard deviation (SD) of triplicates. GraphPad InStat was used to determine whether a difference was statistically significant employing one-way ANOVA followed by a Tukey multiple range test.

Results & discussion

UV–visible spectroscopy of ZnONPs

To establish that ZnONPs were produced biogenically, UV–visible spectroscopic investigation was undertaken. The material dissolved in deionized water was subjected to UV–visible scanning in the 300–800 nm range. The presence of ZnONPs in the combination was established by an intense peak at 370 nm (Fig. 2). The mobility of the electronic cloud on the basic skeleton of ZnONPs may be responsible for the broad absorption band that extends to longer wavelengths.

FTIR analysis of ZnONPs

The FTIR spectra of PPE and ZnONPs were examined to determine whether functional groups associated with these reductive biomolecules exist and to identify the functional groups that specifically contributed to the reduction of ZnO into nanoparticles. Various functional groups can be seen in PPE (Fig. 3). Both the N–H stretching vibration for amino and phenolic hydroxyl groups showed broad band at 3247 cm^{-1}. The peak at 2932 cm^{-1} may be assigned to C–H stretching vibrations to $–CH_3$ and $=CH_2$. At 1666–1612 cm^{-1}, a prominent band of the carboxylic acid stretch was detected, and the peaks at 1407 cm^{-1} and 1027 cm^{-1} may be attributed to –C–O– stretching and vibration, respectively. These distinctive peaks demonstrate the

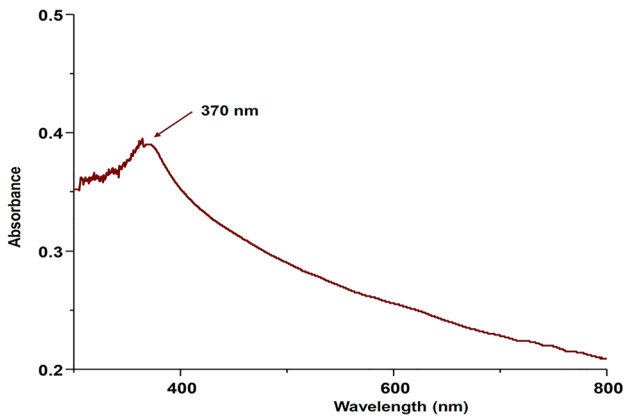

Fig. 2 UV–visible spectra of ZnONPs synthesized using PPE

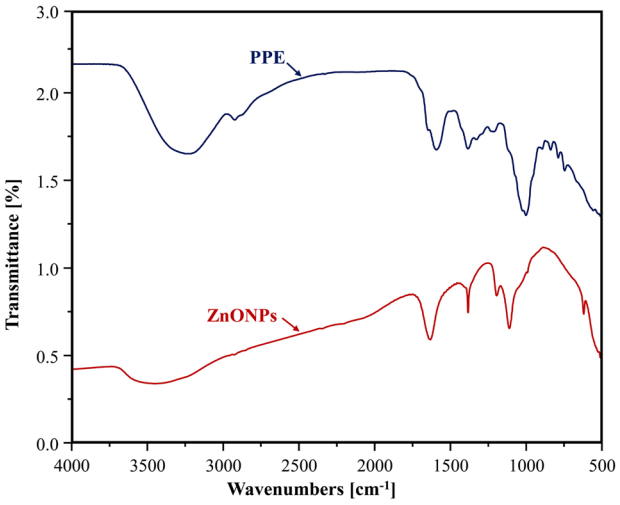

Fig. 3 FTIR spectroscopy of PPE and ZnONPs

presence of polyphenolic chemicals in the extract, which may function as a bio-reductant in the oxidation of ZnO to generate ZnONPs [35]. Flavonoids, proanthocyanidins, simple phenolics, and their derivatives present in PPE might be involved in the creation of nanoparticles and the reduction of metal or metal oxide ions into them [36]. The presence of polyphenolic compounds on the surfaces of nanoparticles is indicated by the FTIR spectra of ZnONPs, which displayed unique peaks at 3447 cm^{-1}, 1633 cm^{-1}, and 1384 cm^{-1} for –OH stretching and stretching vibration of –C = O and –O–C–, respectively. Besides, stretching of –C–O showed another peak at 1111 cm^{-1}. The formation of ZnONPs was confirmed by the peaks at 620 cm^{-1} and 482 cm^{-1} attributed to a –O–H bond between the oxygen atoms of ZnO.

XRD analysis of ZnONPs

XRD analysis was used to validate the biosynthesis of pure and crystalline ZnONPs. Figure 4 displays the analysis's Miller indices peaks, which can be used to identify the hexagonal wurtzite phase structure supported by JCDPS Cardno.89–1397 [37]. X-ray diffraction analysis revealed the 2θ distinctive peaks of ZnONPs at 32.06°, 34.56°, 36.19°, 47.48°, 56.72°, 63.05°, 66.38°, 67.99°, 69.45°, 72.61°, and 77.12° represent the (100), (002), (101), (102), (110), (103), (200), (112), (201), (004), and (202) Bragg's reflections of the face-centered cubic structure of zinc, respectively. The narrow and strong diffraction peaks show the optimal crystalline structure of ZnONPs. However, the absence of noise to significant extent indicates that the synthesized nanoparticles were free from contaminants.

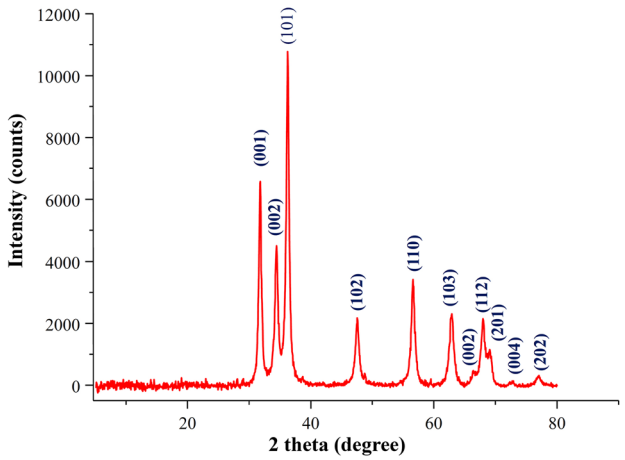

Fig. 4 XRD patterns of ZnONPs

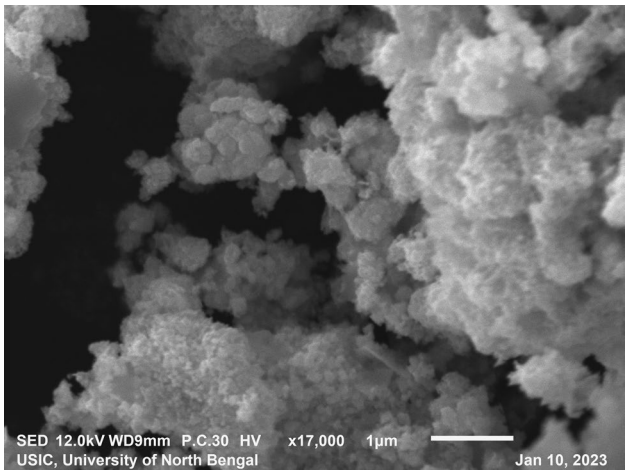

Fig. 5 SEM image of ZnONPs

Particle size and zeta potential analysis of ZnONPs

Particle size analysis by Zetasizer revealed the hydrodynamic diameter of ZnONPs was 170.67 nm (Fig. S1a). The electrical potential that surrounds a charged particle in the hydrodynamic plane of shear is known as the zeta potential. The dispersion is stable when all of the particles have a significant positive or negative zeta potential (where the positivity and negativity are higher or lower than + 30 mV and − 30 mV). In this case, the particles will repel one another to prevent aggregation [38, 39]. On the other hand, if the zeta potential values of the particles are low, there will not be enough force to stop the particles from aggregating. The zeta potential value of ZnONPs of − 21.0 mV (Fig. S1b) confirms their stability in lyophilized form.

SEM of ZnONPs

The nanostructure and morphology of the PPE-derived ZnONPs nanoparticles was evaluated by SEM. The particles show formation of varying shapes and sizes, uniform distribution, loose aggregates, and high porosity (Fig. 5). Even inside the aggregates, there is no direct contact between the nanoparticles, which is a sign of stabilization.

TEM of ZnONPs

TEM micrographs were used to examine the shape and particle size of pure ZnONPs. As shown in Fig. 6, the presence of spherical- to hexagonal-shaped particles was observed.

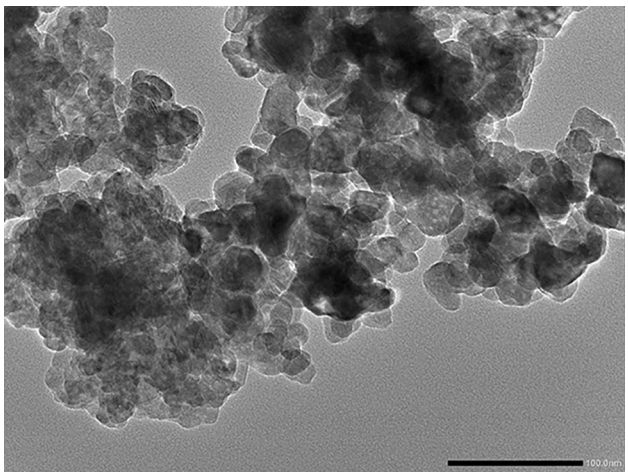

Fig. 6 TEM image of ZnONPs

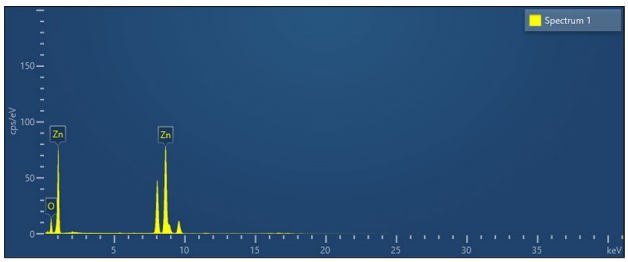

Fig. 7 EDX spectrum of ZnONPs

EDX analysis of ZnONPs

EDX was used to determine the sample's exploration in order to extend secondary vision into the topographies of ZnONPs. According to the EDX analysis (Fig. 7) principal

elements present in ZnONPs were zinc and oxygen.The EDX spectra showed two strong zinc peaks at 1 keV and 8.7 keV, respectively, and a single oxygen peak at ~0.5 keV, all characteristic of ZnONPs. High intensity zinc and oxygen peaks indicate that the sample is primarily made up of zinc oxide.

In vitro antioxidant assay of extract and ZnONPs

DPPH radical scavenging activity of PPE and ZnONPs

In vitro DPPH radical scavenging potential helps determine free radical neutralizing capacity of test material by donating hydrogen. The DPPH radical scavenging activity of PPE, ZnONPs, and ascorbic acid are depicted in Fig. 8a. Although ascorbic acid had a greater ability to scavenge free radicals, both PPE and ZnONPs neutralized DPPH radical in a concentration-dependent manner (25–150 µg/ml). IC_{50} values were found to be 115.13 µg/ml, 98.74 µg/ml, and 39.57 µg/ml for PPE, ZnONPs, and ascorbic acid, respectively.

FRAP of PPE and ZnONPs

The antioxidant property of a test material can be estimated in vitro by its ability to convert ferric iron (Fe^{3+}) to ferrous iron (Fe^{2+}) by donating an electron or hydrogen. Figure 8b represents the reducing power of PPE, ZnONPs, and ascorbic acid according to their concentration. In this study, all the test materials showed a concentration-dependent increase in Fe^{3+} reduction potential (25–150 µg/ml). However, the Fe^{3+} reduction potential of ascorbic acid remained higher than PPE and ZnONPs.

Considering DPPH radical scavenging potential and Fe^{3+} reduction potential, it can be said that green synthesized ZnONPs showed improved antioxidant potential compared to crude PPE.

Antibacterial activity of ZnONPs

The synthesized ZnONPs showed inhibitory activity against selective Gram-positive as well as Gram-negative test organisms. Results from the disc diffusion assay (Fig. S2) are displayed in Table 1. PPE did not show any zone of inhibition at the concentration of 500 µg/ml. However, ZnONPs exhibited significant antibacterial effects against the tested bacterial strains. The effect was found to be highest against *E. coli* followed by *B. subtilis*, S. *Typhi,* and *S. aureus*.

The MICs for the ZnONPs against *S. aureus*, *B. subtilis*, *E. coli, and S. Typhi* were found to be 600, 540, 330, and 510 µg/ml, respectively. However, the antibacterial potential of ZnONPs was more pronounced against Gram-negative bacteria compared to Gram-positive bacteria evidenced by MIC values and inhibited zone diameters.

Photocatalytic activity of ZnONPs

A typical water-soluble dye, rhodamine B, is utilized to evaluate photocatalytic activity of a substance under sunlight. The degradation of rhodamine B in the presence of ZnONPs was measured spectrophotometrically. Rhodamine B shows typical maximum absorption peak at 554 nm. The steady change in color from deep pink to a colorless solution indicates dye degradation. The degradation of the dyes in the presence of PPE and ZnONPs is illustrated in Fig. 9, where

Table 1 Zone of inhibition of ZnONPs and streptomycin

Microorganism	Zone diameter (mm)	
	ZnONPs (500 µg/ml)	Streptomycin (500 µg/ml)
S. aureus	4.67 ± 0.58	17.33 ± 0.57
B. subtilis	9.66 ± 2.31	16.00 ± 1.00
E. coli	14.00 ± 1.00	32.33 ± 0.57
S. typhi	9.33 ± 0.58	18.00 ± 1.00

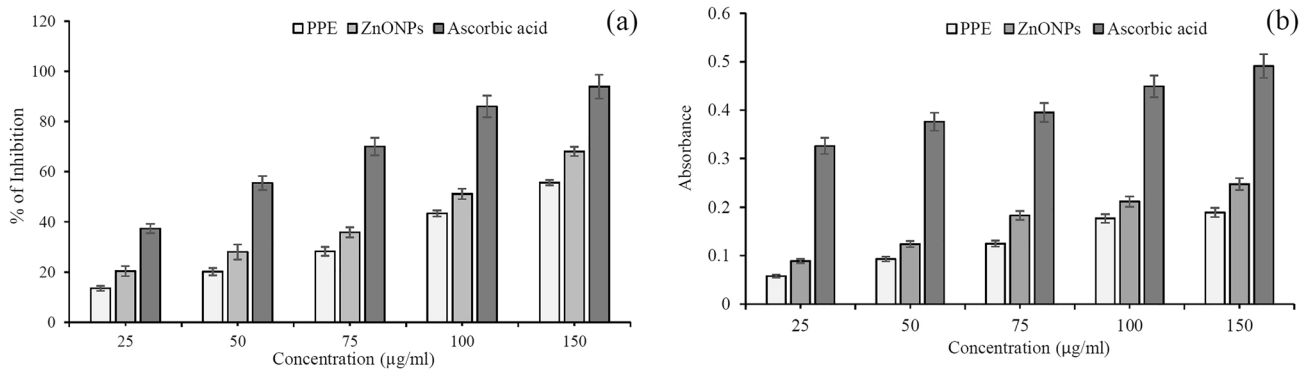

Fig. 8 DPPH radical scavenging activity (**a**) and FRAP (**b**) of PPE, ZnONPs, and ascorbic acid

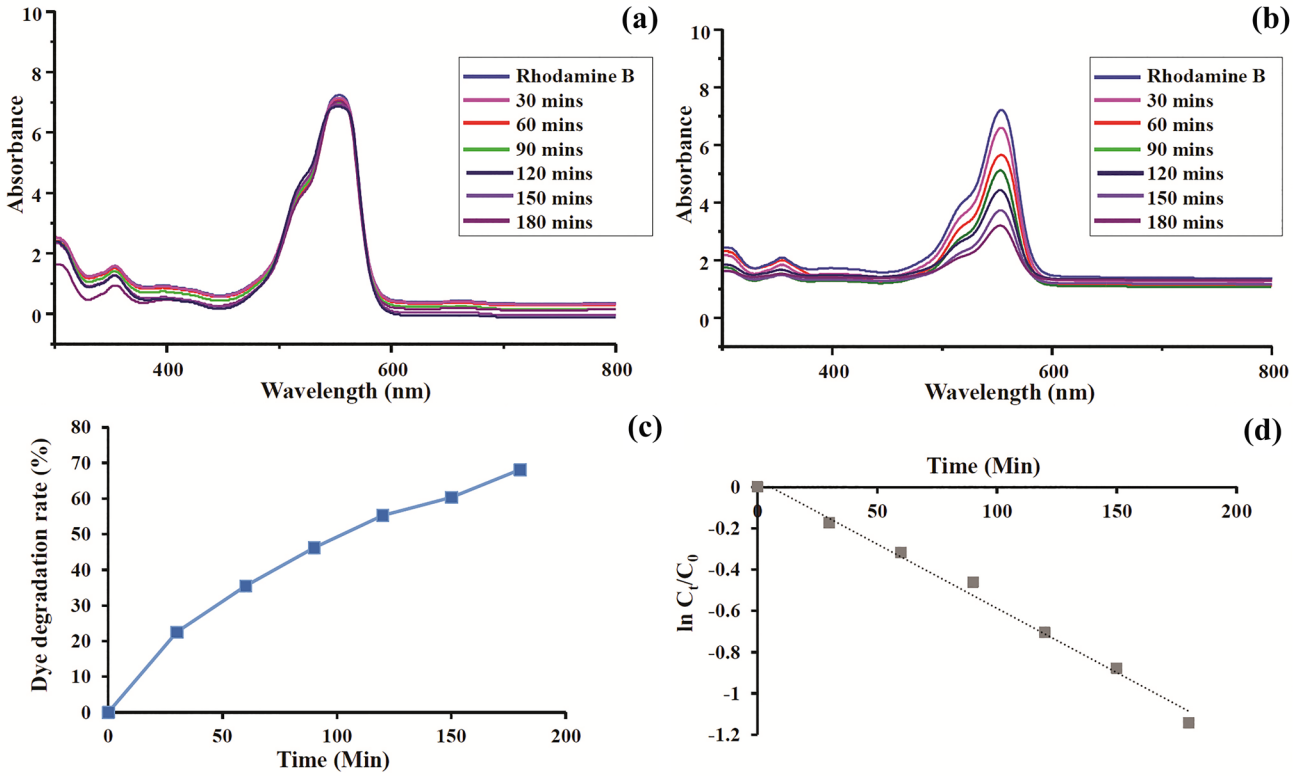

Fig. 9 Photocatalytic activities of PPE (**a**), ZnONPs (**b**), rhodamine B degradation rate in the presence of ZnONPs (**c**) and kinetic plot of degradation of rhodamine B in the presence of ZnONPs (**d**)

it is clearly seen that the rhodamine B absorption band gradually decreases over time and eventually approaches the baseline.

The steady change in color from a bright pink to a colorless solution indicates that the dye is degrading. PPE does not show any degradation of rhodamine B with time (Fig. 9a), whereas rhodamine B in the presence of ZnONPs showed an accelerated rate of photodegradation with time (Fig. 9b). At 180 min, there was a considerable photodegradation (67.1%) of the rhodamine B dye (Fig. 9c). Figure 9d shows the ln (C_t/C_0) vs. time curve for rhodamine B. The measured degradation rate constant of rhodamine B was found to be 1.24×10^{-2}/min. The fact that Ln (C_t/C_0) value declined over time shows that the reaction process was pseudo-first-order kinetic.

Conclusion

This research led to a nature-friendly development of ZnONPs using papaya fruit peels, an underused food waste. The green synthesized nanoparticles showed notable antioxidant potential at a concentration range of 25–150 µg/ml. The ZnONPs showed good antibacterial effects against human pathogens (*S. Typhi, B. subtilis, S. aureus,* and *E. coli*) at the concentrations significantly higher than the concentration they exhibited antioxidant effect. Thus, it might be said that the bacteria inhibitory potential could be associated with the prooxidant effect of ZnONPs at higher concentration. Both antioxidant and prooxidant effects could be effectively used for therapeutic purposes in different ailments. In addition, ZnONPs exhibited an excellent photocatalytic activity. Thus, this study provides a product of versatile applications in pharmaceutical, chemical, and biomedical industries. Furthermore, the utilization of a fruit waste for developing a commercial product might open a novel opportunity of food-derived waste management in future.

Supplementary Information The online version contains supplementary material available at https://doi.org/10.1007/s00449-023-02945-7.

Acknowledgements The authors sincerely acknowledge the University of North Bengal, India, for providing support and facilities to conduct this work.

Funding Not applicable.

Data availability The authors declare that the data supporting the findings of this study are available within the paper and its Supplementary Information files.

Declarations

Conflict of interest The authors declare that they do not have any conflict of interest.

References

1. Noukelag S, Mohamed H, Moussa B, Razanamahandry L, Ntwampe SKO, Arendse C, Maaza M (2020) Investigation of structural and optical properties of biosynthesized Zincite (ZnO) nanoparticles (NPs) via an aqueous extract of Rosmarinus officinalis (rosemary) leaves. MRS Adv 5:2349–2358
2. Vayssieres L (2004) On the design of advanced metal oxide nanomaterials. Int J Nanotechnol 1:1–41
3. Shoeb M, Singh BR, Khan JA, Khan W, Singh BN, Singh HB, Naqvi AH (2013) ROS-dependent anticandidal activity of zinc oxide nanoparticles synthesized by using egg albumen as a biotemplate. Adv Natl Sci: Nanosci Nanotechnol 4:035015
4. Jayappa MD, Ramaiah CK, Kumar MAP, Suresh D, Prabhu A, Devasya RP, Sheikh S (2020) Green synthesis of zinc oxide nanoparticles from the leaf, stem and in vitro grown callus of *Mussaenda frondosa* L.: characterization and their applications. Appl Nanosci 10:3057–3074
5. Janotti A, Van de Walle CG (2009) Fundamentals of zinc oxide as a semiconductor. Rep Prog Phys 72:126501
6. Kolodziejczak-Radzimska A, Jesionowski T (2014) Zinc oxide-from synthesis to application: a review. Materials (Basel) 7:2833–2881
7. Das D, Nath BC, Phukon P, Dolui SK (2013) Synthesis of ZnO nanoparticles and evaluation of antioxidant and cytotoxic activity. Colloids Surf, B 111:556–560
8. Li C, Liu H, Sun Y, Wang H, Guo F, Rao S, Deng J, Zhang Y, Miao Y, Guo C (2009) PAMAM nanoparticles promote acute lung injury by inducing autophagic cell death through the Akt-TSC2-mTOR signaling pathway. J Mol Cell Biol 1:37–45
9. Premanathan M, Karthikeyan K, Jeyasubramanian K, Manivannan G (2011) Selective toxicity of ZnO nanoparticles toward Gram-positive bacteria and cancer cells by apoptosis through lipid peroxidation. Nanomed: Nanotechnol Biol Med 7:184–192
10. Prabhu YT, Rao KV, Kumar VSS, Kumari BS (2013) Synthesis of ZnO nanoparticles by a novel surfactant assisted amine combustion method. Adv Nanopart 2:45
11. Usui H, Shimizu Y, Sasaki T, Koshizaki N (2005) Photoluminescence of ZnO nanoparticles prepared by laser ablation in different surfactant solutions. J Phys Chem B 109:120–124
12. Kavitha G, Arul KT, Babu P (2018) Enhanced acetone gas sensing behavior of n-ZnO/p-NiO nanostructures. J Mater Sci: Mater Electron 29:6666–6671
13. Thovhogi N, Diallo A, Gurib-Fakim A, Maaza M (2015) Nanoparticles green synthesis by *Hibiscus sabdariffa* flower extract: main physical properties. J Alloy Compd 647:392–396
14. Barzinjy AA, Azeez HH (2020) Green synthesis and characterization of zinc oxide nanoparticles using *Eucalyptus globulus* Labill. leaf extract and zinc nitrate hexahydrate salt. SN Appl Sci 2:991
15. Akintelu SA, Folorunso AS (2020) A review on green synthesis of zinc oxide nanoparticles using plant extracts and its biomedical applications. BioNanoScience 10:848–863
16. Rastogi A, Singh P, Haraz FA, Barhoum A (2018) Biological synthesis of nanoparticles: an environmentally benign approach. Fundamentals of nanoparticles. Elsevier, Amsterdam
17. Kokila T, Ramesh P, Geetha D (2016) Biosynthesis of AgNPs using *Carica Papaya* peel extract and evaluation of its antioxidant and antimicrobial activities. Ecotoxicol Environ Saf 134:467–473
18. Ang YK, Sia WC, Khoo HE, Yim HS (2012) Antioxidant potential of *Carica papaya* peel and seed. Focus Modern Food Ind 1:11–16
19. Sharma A, Bachheti A, Sharma P, Bachheti RK, Husen A (2020) Phytochemistry, pharmacological activities, nanoparticle fabrication, commercial products and waste utilization of *Carica papaya* L.: a comprehensive review. Curr Res Biotechnol 2:145–160
20. Singh SP, Kumar S, Mathan SV, Tomar MS, Singh RK, Verma PK, Kumar A, Kumar S, Singh RP, Acharya A (2020) Therapeutic application of Carica papaya leaf extract in the management of human diseases. Daru: J Fac Pharm, Tehran Univ Med Sci 28:735–744
21. Pathak PD, Mandavgane SA, Kulkarni BD (2019) Waste to wealth: a case study of papaya peel. Waste Biomass Valoriz 10:1755–1766
22. Singh PK, Rawat P (2017) Evolving herbal formulations in management of dengue fever. J Ayurveda Integr Med 8:207–210
23. Thema F, Manikandan E, Dhlamini M, Maaza M (2015) Green synthesis of ZnO nanoparticles via Agathosma betulina natural extract. Mater Lett 161:124–127
24. Suresh D, Shobharani R, Nethravathi P, Kumar MP, Nagabhushana H, Sharma S (2015) Artocarpus gomezianus aided green synthesis of ZnO nanoparticles: luminescence, photocatalytic and antioxidant properties. Spectrochim Acta Part A Mol Biomol Spectrosc 141:128–134
25. Jiang C, Zhao L, Li S, Zhao X, Zhang Q, Xiong Q (2013) Preliminary characterization and immunostimulatory activity of polysaccharides from Glossaulax didyma. Food Chem Toxicol 62:226–230
26. Khan A, Rashid A, Younas R, Chong R (2016) A chemical reduction approach to the synthesis of copper nanoparticles. Int Nano Lett 6:21–26
27. López-Miranda JL, Esparza R, González-Reyna MA, España-Sánchez BL, Hernandez-Martinez AR, Silva R, Estévez M (2021) Sargassum influx on the Mexican Coast: a source for synthesizing silver nanoparticles with catalytic and antibacterial properties. Appl Sci 11:4638
28. Ying Z, Han X, Li J (2011) Ultrasound-assisted extraction of polysaccharides from mulberry leaves. Food Chem 127:1273–1279
29. Shanmuganathan R, Sathishkumar G, Brindhadevi K, Pugazhendhi A (2020) Fabrication of naringenin functionalized-Ag/RGO nanocomposites for potential bactericidal effects. J Market Res 9:7013–7019
30. Ajitha B, Reddy YAK, Reddy PS (2015) Green synthesis and characterization of silver nanoparticles using *Lantana camara* leaf extract. Mater Sci Eng, C 49:373–381
31. Mensor LL, Menezes FS, Leitão GG, Reis AS, Santos TCd, Coube CS, Leitão SG (2001) Screening of Brazilian plant extracts for antioxidant activity by the use of DPPH free radical method. Phytother Res 15:127–130
32. Oyaizu M (1986) Studies on products of browning reaction antioxidative activities of products of browning reaction prepared from glucosamine. Japan J Nutr Diet 44:307–315
33. Haydar MS, Das D, Ghosh S, Mandal P (2022) Implementation of mature tea leaves extract in bioinspired synthesis of iron oxide nanoparticles: preparation, process optimization, characterization, and assessment of therapeutic potential. Chem Pap 76:491–514
34. Ravichandran V, Vasanthi S, Shalini S, Shah SAA, Tripathy M, Paliwal N (2019) Green synthesis, characterization, antibacterial, antioxidant and photocatalytic activity of *Parkia speciosa* leaves extract mediated silver nanoparticles. Results Phys 15:102565
35. Saad Algarni T, Abduh NA, Al Kahtani A, Aouissi A (2022) Photocatalytic degradation of some dyes under solar light irradiation using ZnO nanoparticles synthesized from Rosmarinus officinalis extract. Green Chem Lett Rev 15:460–473

36. Supraja N, Prasad T, Krishna TG, David E (2016) Synthesis, characterization, and evaluation of the antimicrobial efficacy of Boswellia ovalifoliolata stem bark-extract-mediated zinc oxide nanoparticles. Appl Nanosci 6:581–590
37. Karaköse E, Çolak H, Duman F (2017) Green synthesis and antimicrobial activity of ZnO nanostructures *Punica granatum* shell extract. Green Process Synth 6:317–323
38. Paul P, Sengupta S, Mukherjee B, Shaw TK, Gaonkar RH, Debnath MC (2018) Chitosan-coated nanoparticles enhanced lung pharmacokinetic profile of voriconazole upon pulmonary delivery in mice. Nanomedicine (Lond) 13:501–520
39. Zając M, Kotyńska J, Zambrowski G, Breczko J, Deptuła P, Cieśluk M, Zambrzycka M, Święcicka I, Bucki R, Naumowicz M (2023) Exposure to polystyrene nanoparticles leads to changes in the zeta potential of bacterial cells. Sci Rep 13:9552

Authors and Affiliations

Serina Easmin[1] · Moulik Bhattacharyya[1] · Krishna Pal[1] · Priya Das[1] · Ranabir Sahu[1] · Gouranga Nandi[1] · Saikat Dewanjee[2] · Paramita Paul[1] · Md Salman Haydar[3] · Swarnendu Roy[3] · Tarun Kumar Dua[1]

✉ Tarun Kumar Dua
tarunkduaju@gmail.com

[1] Department of Pharmaceutical Technology, University of North Bengal, Raja Rammohunpur, P.O.-NBU, Siliguri, West Bengal 734013, India

[2] Advanced Pharmacognosy Research Laboratory, Department of Pharmaceutical Technology, Jadavpur University, Kolkata 700032, India

[3] Plant Biochemistry Laboratory, Department of Botany, University of North Bengal, Raja Rammohunpur, P.O. NBU, Siliguri, West Bengal 734013, India